Optimal Parametric Design of Radial Magnetic Torque Couplers via Dimensional Analysis

Jacob L. B. Aman[1,2], Jake J. Abbott[3], and Shad Roundy[3]

[1]Lawrence Livermore National Laboratory, Livermore, CA 94550 USA
[2]Department of Electrical and Computer Engineering, University of Utah, Salt Lake City, UT 84112 USA
[3]Department of Mechanical Engineering, University of Utah, Salt Lake City, UT 84112 USA

In this article, we apply dimensional analysis to the optimization of radial magnetic torque couplers. Our goal is to find the design that maximizes the torque potential in a given package size. We consider two types of torque coupler: the permanent-magnet (a.k.a. synchronous) torque coupler, in which both the inner and outer rotors contain permanent magnets; and the variable-reluctance torque coupler, in which the inner rotor contains permanent magnets and the outer rotor contains soft-magnetic teeth. Both types of torque coupler are defined by the same set of independent geometric and material parameters. First, the Buckingham Π theorem is used to find the minimal set of dimensionless parameters required for design optimization. Then, using a combination of 2-D and 3-D finite-element analysis, we find and characterize the optimal designs. We explicitly consider torque couplers with eight stable magnetic equilibria (i.e., 45° of rotation between stable equilibria), but the methodology can be repeated for other configurations.

Index Terms— **Magnetic devices, magnetic torque couplers, rotor, stator.**

I. Introduction

A MAGNETIC torque coupler is designed to transmit torque between an inner rotor (IR) and an outer rotor (OR) magnetically, without a mechanical connection, with the torque being a function of the relative displacement of the IR and OR. A magnetic torque coupler comprises one or more stable magnetic equilibria, with a nonlinear magnetic spring binding the IR and OR at each equilibrium. In a *radial* magnetic torque coupler, the magnetic flux between the IR and OR is largely in the radial direction (i.e., orthogonal to the axis of rotation). There are two types of radial magnetic torque couplers: the most common type is the permanent-magnet torque coupler, in which both the IR and OR contain permanent magnets; and the less-explored type is the variable-reluctance torque coupler, in which the IR contains permanent magnets and the OR contains soft-magnetic teeth [1], [2]. Both types of torque coupler typically include an outer soft-magnetic yoke in the OR and an inner soft-magnetic core in the IR.

For all of the efforts in the literature dedicated to modeling and optimizing radial magnetic torque couplers, the community has still not arrived at a unique optimal design. This is largely due to the complexity of the problem, but also due to varying definitions of optimality. Hornreich and Shtrikman [3] derived an early model to compute the peak torque transmitted by radial couplers, and then used the formula to optimize the design to maximize torque per volume of magnetic material; however, the model was 2-D and made other simplifying assumptions such as assuming infinite permeability of the soft-magnetic yoke. Wu *et al.* [4] showed that 3-D finite-element analysis (FEA) was superior at predicting torque in radial couplers compared to both 2-D FEA and the method of [3] (which are reasonably close to each other but both substantially overestimate torque due to unmodeled flux leakage at the ends of the coupler); they then described how they utilized the 3-D FEA in the optimization of a specific ten-pole-pair coupler. Most recently, Choi *et al.* [5] derived a 3-D model (again assuming infinite permeability of the soft-magnetic yoke) that does a good job of predicting torque in radial couplers (although it still tends to overpredict the torque).

Others have made the assumption of ideal permanent magnets and no other material contributing to the magnetic field (e.g., the soft-magnetic yoke typically used in couplers), which enabled additional results. Furlani *et al.* [6] derived a 3-D model to compute the torque transmitted by radial couplers, and then used that model to perform design optimization [7]. Charpentier and Lemarquand [8] extended this type of 3-D formula to consider magnets with a more complex polarization patterns (i.e., radial and tangential); a similar result can be realized using Halbach arrays [9]. Ravaud *et al.* [10] improved on this model to more accurately capture the arc shape of the permanent magnets commonly used in couplers. Meng *et al.* [11] then improved on this model by generalizing to any number of magnetic pole pairs, and found reasonable agreement with 3-D FEA results (the soft-magnetic yoke was included in the FEA, although it was not included in the model).

Many researchers have noted the inefficiency of performing design optimization using exhaustive FEA simulations, yet 3-D FEA simulations remains the gold standard for design. To address this issue, Lin *et al.* [9] proposed using Taguchi-style design-of-experiments methods to make optimization more efficient. However, the community continues to perform optimization on a case-by-case basis, with a large number of independent design parameters to consider.

Other communities in science and engineering commonly make use of dimensional analysis to find a valid minimum set of dimensionless terms that capture the physics of a given problem, and then conduct simulations and/or experiments

Manuscript received June 22, 2021; revised February 3, 2022; accepted March 13, 2022. Date of publication March 21, 2022; date of current version May 23, 2022. Corresponding author: J. J. Abbott (e-mail: jake.abbott@utah.edu).

Color versions of one or more figures in this article are available at https://doi.org/10.1109/TMAG.2022.3160942.

Digital Object Identifier 10.1109/TMAG.2022.3160942

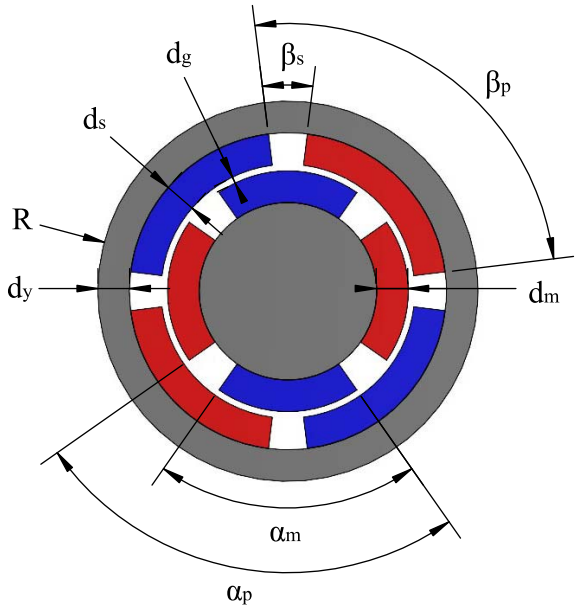

Fig. 1. Geometric parameters defining the cross section of a permanent-magnet torque coupler; see Table I for definitions. Red indicates a permanent magnet magnetized radially outward, and blue indicates magnetization radially inward. For a variable-reluctance torque coupler, the permanent magnets on the OR are replaced with soft-magnetic teeth, but all geometric parameters are maintained.

in those dimensionless terms. This technique has not been utilized in the design of magnetic torque couplers (radial or otherwise). Further, the use of dimensional analysis could have similar benefits to those interested in the design of magnetic gears and other related magnetic devices.

In this article, we apply dimensional analysis to the optimization of radial magnetic torque couplers. Our goal is to find the design that maximizes the torque potential in a given package size, and then report the specifications of that optimal design. We consider both the permanent-magnet torque coupler (Fig. 1) and the variable-reluctance torque coupler. Ultimately, both types of torque coupler are defined by the same set of independent geometric and material parameters, but in the variable-reluctance torque coupler, the OR permanent magnets are replaced with soft-magnetic teeth. Herein, we explicitly consider torque couplers with 45° of rotation between stable equilibria, but the methodology presented here can be repeated for any other design configuration.

II. Dimensional Analysis

Dimensional analysis is a method that relates the governing parameters of a problem to physical laws. By finding a functional relationship between these parameters, a complex problem can often be reduced to a simpler one. Dimensional analysis helps minimize the total number of experiments and/or simulations that must be conducted, and it enables the results obtained to be easily generalized and scaled.

We apply a dimensional-analysis technique known as the Buckingham Π theorem [12]. We begin by enumerating all independent parameters that have the potential to affect the given dependent parameter of interest (i.e., torque). For our problem, these include geometric parameters (i.e., lengths and angles) and material properties defining the permanent-magnet and soft-magnetic materials (note that the soft-magnetic material is sometimes referred to as electrical steel in this context). A total of six length parameters are used: five that define the cross section shown in Fig. 1; as well as the length of the torque coupler, L, normal to the cross section. There are two angular parameters that define the cross section, which are represented as nondimensional fractions of an angle: one is the arc angle of an OR slot divided by the combined arc angle of an OR magnet (or OR tooth) and OR slot, $E = \beta_s/\beta_p$; the other is the arc angle of an IR magnet divided by the combined arc angle of an IR magnet and an IR slot, $F = \alpha_m/\alpha_p$. A linear model is used to represent the permanent-magnet material [13], which requires two parameters: the coercivity H_{cm} and permeability μ_m. Finally, the soft-magnetic material in the yoke and IR core, as well as in the OR teeth in the case of a variable-reluctance torque coupler, is defined by two parameters: the permeability μ_y (up to saturation) and the saturation flux density B_y.

With a total of 13 governing parameters (one dependent and 12 independent), and three independent dimensions (m, N, A), we expect a total of $13 - 3 = 10$ dimensionless Π groups (see Table I), to fully capture the physics of the problem with $\Pi_0 = f(\Pi_1, \ldots, \Pi_9)$. To choose the three linearly independent parameters representing the three independent dimensions, we select the outer radius R (which effectively

TABLE I

Torque and the 12 Independent Parameters That Affect It. The Nondimensionalized Torque, Π_0, Can Be Expressed as a Function of Just Nine Dimensionless Π Groups, Π_1–Π_9. IR Indicates Inner Radius and OR Indicates Outer Radius

Parameter	Symbol	Dimension	Π Group
Torque	T	N·m	$\Pi_0 = \frac{T}{\mu_m H_{cm}^2 R^3}$
Length	L	m	$\Pi_1 = \frac{L}{R}$
Outer Radius	R	m	
IR Magnet Thickness	d_m	m	$\Pi_2 = \frac{d_m}{R}$
Air-gap Thickness	d_g	m	$\Pi_3 = \frac{d_g}{R}$
OR Slot Depth	d_s	m	$\Pi_4 = \frac{d_s}{R}$
Yoke Thickness	d_y	m	$\Pi_5 = \frac{d_y}{R}$
OR Fractional Slot Arc Angle	E	—	$\Pi_6 = E$
IR Fractional Magnet Arc Angle	F	—	$\Pi_7 = F$
Soft-magnetic Permeability	μ_y	$\frac{\mathrm{N}}{\mathrm{A}^2}$	$\Pi_8 = \frac{\mu_y}{\mu_m}$
Soft-magnetic Saturation	B_y	$\frac{\mathrm{N}}{\mathrm{A{\cdot}m}}$	$\Pi_9 = \frac{B_y}{\mu_m H_{cm}}$
Permanent-magnet Permeability	μ_m	$\frac{\mathrm{N}}{\mathrm{A}^2}$	
Permanent-magnet Coercivity	H_{cm}	$\frac{\mathrm{A}}{\mathrm{m}}$	

represents the dimension m), the permanent-magnet coercivity $H_{\rm cm}$ (which effectively represents the dimension A, linearly independent of R), and the permanent-magnet permeability μ_m (which effectively represents the dimension N, linearly independent of R and $H_{\rm cm}$). We then use R, μ_m, and $H_{\rm cm}$ to nondimensionalize the nine remaining parameters. Note that E and F are already in a dimensionless form. The Π terms that we created are not unique, but we can verify that we have selected a valid set using the method described in Appendix A. Using 3-D FEA (Ansys), we verified our nondimensionalization by: 1) changing values of μ_m, $H_{\rm cm}$, and R one a time; 2) changing all other parameters to maintain constant Π_1–Π_9; and 3) verifying that Π_0 remained constant.

The form of Π_0 (see Table I) indicates that we should expect torque T to scale linearly with μ_m, quadratically with $H_{\rm cm}$, and cubicly with R, provided Π_1–Π_9 are held constant. This was known before any actual simulations were performed, but we also verified it, as described above. Note that changing R^3 while holding $\Pi_1 = L/R$ constant is effectively changing the volume of the magnetic torque coupler without changing the aspect ratio. Also, note that $\mu_m H_{\rm cm}^2$ is referred to as the energy product of a permanent-magnet material. Thus, the form of Π_0, which fell out of the Buckingham Π theorem, is intuitive based on first principles.

III. Designing the Number of Magnetic Equilibria

A magnetic torque coupler can be designed with any positive-integer number Z of stable magnetic equilibria; Z is also the number of full periods of the torque waveform as the IR completes one full rotation with respect to the OR. This choice results in a mechanical angle of

$$\phi = \frac{360^\circ}{Z} = \frac{2\pi}{Z} \text{ rad} \tag{1}$$

between stable magnetic equilibria. Here, for a desired Z, we review how to choose the number of IR and OR magnets in the case of permanent-magnet torque couplers, and we describe a method to choose the number of IR magnets and OR teeth in the case of variable-reluctance torque couplers.

A. Permanent-Magnet Torque Coupler

It is common practice to design permanent-magnet torque couplers with the same number of IR and OR magnets [3]–[9], with alternating magnetic polarity, and this number is always an even integer described by

$$N_{\rm IR} = N_{\rm OR} = 2Z. \tag{2}$$

For $Z = 8$ (our case study in this article), which has $\phi = 45^\circ$ between stable equilibria, $N_{\rm IR} = N_{\rm OR} = 16$.

B. Variable-Reluctance Torque Coupler

Best practice has not yet been established for variable-reluctance torque couplers. The torque in a variable-reluctance torque coupler is fundamentally the same as the cogging torque in a brushless dc motor. Our ultimate goal is to maximize torque. To this end, we have identified a method intended to minimize cogging torque in motors [14], and we repurpose it here to maximize torque in variable-reluctance torque couplers.

For a variable-reluctance torque coupler with $N_{\rm IR}$ magnets and $N_{\rm OR}$ teeth, z describes the number of periods of the torque waveform resulting from the IR being rotated by β_p with respect to the OR (i.e., by one tooth-slot pair, referred to as the pitch, see Fig. 1)

$$z = \frac{N_{\rm IR}}{\text{HCF}(N_{\rm IR}, N_{\rm OR})} \tag{3}$$

where HCF is the highest-common-factor function. $z = 1$ is the lowest period that can be achieved and indicates a design in which the edges of all magnets interact with the edges of all teeth simultaneously. A z value greater than one indicates that the magnet edges interact with the teeth edges asynchronously. The number of stable magnetic equilibria is

$$Z = zN_{\rm OR}. \tag{4}$$

To maximize the peak torque, we should select a design with the lowest value of z (i.e., $z = 1$) to maximize torque [14]. This results in a unique choice for selecting the number of OR teeth

$$N_{\rm OR} = Z. \tag{5}$$

However, there may be more than one value of $N_{\rm IR}$ that result in $z = 1$. We will show in Section IV that $N_{\rm IR}$ should be chosen as large as possible.

For $Z = 8$ (our case study in this article), which has $\phi = 45^\circ$ between stable equilibria, $N_{\rm OR} = 8$. Any of $N_{\rm IR} = 2$, $N_{\rm IR} = 4$, or $N_{\rm IR} = 8$ result in $z = 1$. We will show that the largest $N_{\rm IR}$ (i.e., $N_{\rm IR} = 8$) maximizes the peak torque.

IV. Design Optimization Using 2-D FEA

In Section III we identified four designs for optimization, all of which provide eight stable magnetic equilibria: one permanent-magnet and three variable-reluctance. We performed optimization for each of these four designs in 2-D FEA, using both Finite Element Method Magnetic (FEMM) [15] and Ansys, which assumes a length $L \to \infty$ and then calculates the torque per unit length. In both FEMM and Ansys, built-in meshing algorithms were used. Ansys uses adaptive meshing that includes a convergence criterion; convergence was typically reached within three iterations. The meshing used in FEMM is not adaptive. However, we found that 2-D FEMM simulation results closely matched those obtained from Ansys, to within a few percent. An example result of a 2-D FEA performed in Ansys is shown in Fig. 2

For our permanent-magnet material, we used $\mu_m = 1.046\mu_0$ (where $\mu_0 = 4\pi \times 10^{-7}$ N $\cdot$ A^{-2} is the permeability of free space) and $H_{\rm cm} = 1.027 \times 10^6$ A$\cdot$m^{-1}, which corresponds to a Grade N45SH NdFeB magnet. For our soft-magnetic material, we used $\mu_y = 1.5 \times 10^4 \mu_0$ and $B_y = 2.35$ N$\cdot$A$^{-1}\cdot$m^{-1}, which corresponds to a CoFe alloy called VACOFLUX 50. These result in constant values of $\Pi_8 = 1.43 \times 10^4$ and $\Pi_9 = 1.74$. The optimization will always try to drive the air gap thickness d_g as small as possible (i.e., to zero), but in practice, there will need to be some small gap; we simply constrained $\Pi_3 = d_g/R = 0.01$. We will return to these assumptions later.

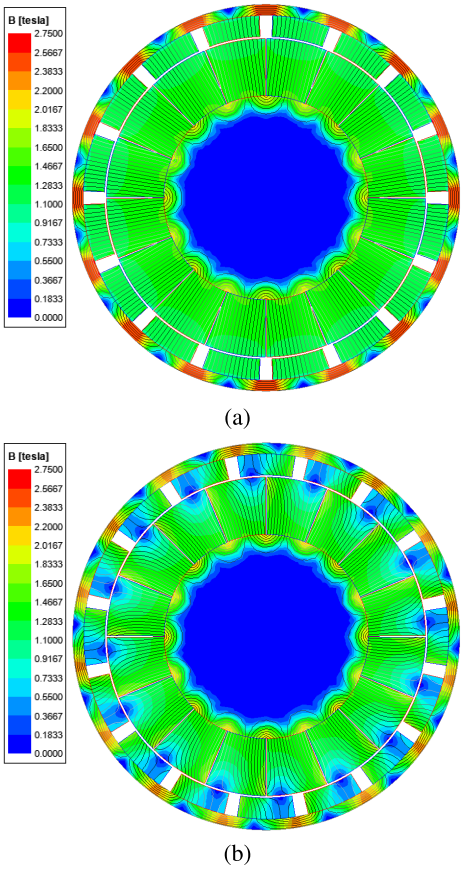

Fig. 2. Example of 2-D FEA showing the magnetic flux density with the rotors shown at (a) zero torque and (b) peak torque. This example depicts the optimal permanent-magnet torque coupler using VACOFLUX 50 for the soft-magnetic material. (a) Rotors aligned: zero torque. (b) Rotors offset by 11:25°: peak torque.

Optimization was performed by searching over the 5-D parameter space including Π_2 and Π_4–Π_7. We first performed a coarse search covering the design space, consisting of all combinations of four levels of each Π term, resulting in 1024 unique designs. For each design, we rotated the IR with respect to the OR in increments of 1° and computed the torque in each configuration, recording the peak torque as shown in Figs. 2 and 3. We then moved forward using the design with the largest peak torque, which we used to seed a constrained optimization function, which we implemented using MATLAB's `FMINCON`. A linear inequality constraint ensured that the IR fits within the OR

$$d_m \leq R - d_y - d_s - d_g. \tag{6}$$

The nondimensional torque waveforms for the four resulting designs are shown in Fig. 4. We see that each waveform has a different shape from the others; all have stable and unstable magnetic equilibria at the same rotation angles, but they experience peak torque at different rotation angles. We see that, when it comes to variable-reluctance torque couplers, we should choose the design with the highest number of IR magnets (from the viable candidates). However, we also see that the peak torque from an optimal permanent-magnet torque coupler is more than twice as large as the peak torque from

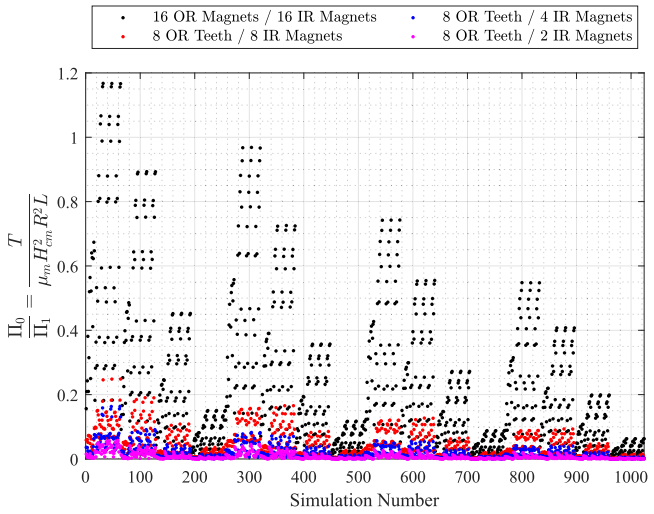

Fig. 3. Peak nondimensional torque for each unique design in the parametric search using VACOFLUX 50 for the soft-magnetic material.

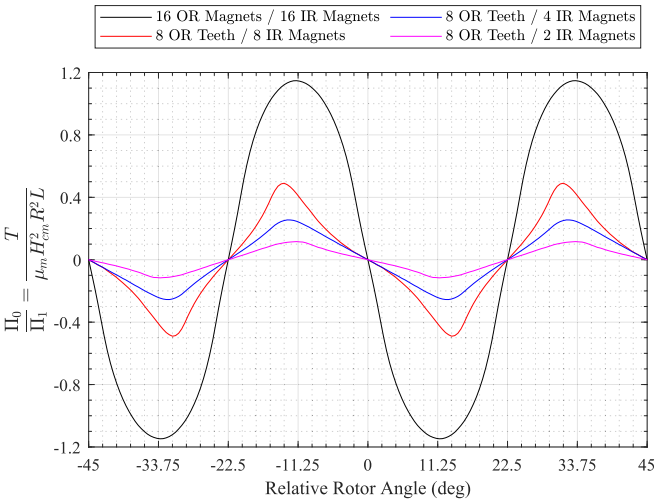

Fig. 4. Nondimensional torque versus relative rotation angle between the IR and OR, for a permanent-magnet torque coupler and three variable-reluctance torque couplers, all with 45° between stable equilibria and using VACOFLUX 50 for the soft-magnetic material. Results were obtained from 2-D FEA, which assumes $L/R \to \infty$. IR indicates inner radius and OR indicates outer radius.

an optimal variable-reluctance torque coupler for the same package size (i.e., the same value of R and L). The geometric parameters of the optimal designs are provided in Table II and depicted in Fig. 5.

Next, we repeated our entire design optimization process, for only the permanent-magnet torque coupler, using 1010 Steel as the soft-magnetic material, which is commonly used in magnetic devices such as this. The results are provided in Table III. As we compare the results using 1010 Steel to those using VACOFLUX 50, we find that the optimal designs of the OR are slightly different as we might expect, yet the optimal designs of the IR are the same. We also find that VACOFLUX 50 results in a peak torque that is 3.5% higher than that of 1010 Steel.

TABLE II

OPTIMAL DESIGN PARAMETERS FOR PERMANENT-MAGNET AND VARIABLE-RELUCTANCE MAGNETIC TORQUE COUPLERS WITH 45° BETWEEN STABLE EQUILIBRIA. RESULTS WERE OBTAINED FROM 2-D FEA (WHICH ASSUMES $L/R \to \infty$) WITH THE FOLLOWING TERMS HELD CONSTANT: $d_g/R = 0.01$, $\mu_m = 1.046\mu_0$, $H_{\rm cm} = 1.027 \times 10^6$ A $\cdot$ m^{-1}, AND USING VACOFLUX 50 AS THE SOFT-MAGNETIC MATERIAL (NOMINAL $\mu_y = 1.5 \times 10^4 \mu_0$ AND $B_y = 2.35$ N $\cdot$ A^{-1} $\cdot$ m^{-1})

Π Group	**Permanent-magnet** ($N_{OR} = 16$, $N_{IR} = 16$)	**Variable-reluctance** ($N_{OR} = 8$, $N_{IR} = 8$)
$\frac{\Pi_0}{\Pi_1} = \frac{T}{\mu_m H_{cm}^2 R^2 L}$	1.15	0.490
$\Pi_2 = \frac{d_m}{R}$	0.296	0.787
$\Pi_4 = \frac{d_s}{R}$	0.109	0.0806
$\Pi_5 = \frac{d_y}{R}$	0.0573	0.0180
$\Pi_6 = E$	0.185	0.366
$\Pi_7 = F$	0.978	0.980

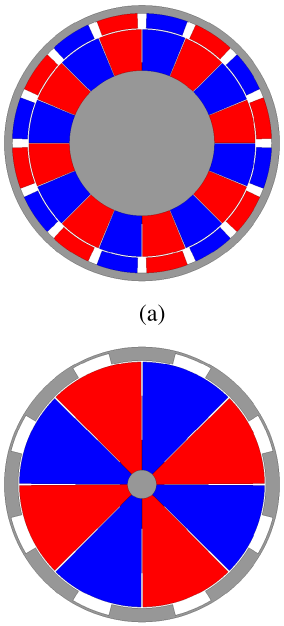

(a)

(b)

Fig. 5. Cross section of optimal magnetic torque couplers with 45° between stable equilibria and using VACOFLUX 50 for the soft-magnetic material, shown at stable equilibria. (a) Optimal permanent-magnet torque coupler. (b) Optimal variable-reluctance torque coupler.

TABLE III

OPTIMAL DESIGN PARAMETERS FOR A PERMANENT-MAGNET MAGNETIC TORQUE COUPLER WITH 45° BETWEEN STABLE EQUILIBRIA. RESULTS WERE OBTAINED FROM 2-D FEA (WHICH ASSUMES $L/R \to \infty$) WITH THE FOLLOWING TERMS HELD CONSTANT: $d_g/R = 0.01$, $\mu_m = 1.046\mu_0$, $H_{\rm cm} = 1.027 \times 10^6$ A $\cdot$ m^{-1}, AND USING 1010 STEEL AS THE SOFT-MAGNETIC MATERIAL (NOMINAL $\mu_y = 2.1 \times 10^3 \mu_0$ AND $B_y = 2.19$ N $\cdot$ A^{-1} $\cdot$ m^{-1})

Π Group	**Permanent-magnet** ($N_{OR} = 16$, $N_{IR} = 16$)
$\frac{\Pi_0}{\Pi_1} = \frac{T}{\mu_m H_{cm}^2 R^2 L}$	1.11
$\Pi_2 = \frac{d_m}{R}$	0.296
$\Pi_4 = \frac{d_s}{R}$	0.099
$\Pi_5 = \frac{d_y}{R}$	0.0511
$\Pi_6 = E$	0.176
$\Pi_7 = F$	0.978

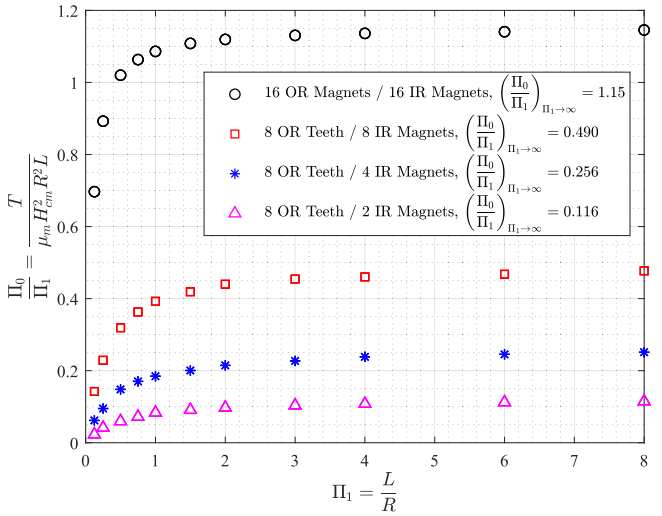

Fig. 6. Peak nondimensional torque versus nondimensional length for the permanent-magnet torque coupler and the three variable-reluctance torque couplers, all with 45° between stable equilibria and using VACOFLUX 50 for the soft-magnetic material. Results were obtained from 3-D FEA. IR indicates inner radius and OR indicates outer radius.

V. CHARACTERIZING LENGTH EFFECTS USING 3-D FEA

2-D FEA tends to overpredict torque in radial magnetic torque couplers because the model does not capture flux leakage at the ends of the device; this effect becomes significant for small values of $\Pi_1 = L/R$. In Fig. 6 we consider the role of Π_1 on peak torque for each of the four optimized designs from Section IV that used VACOFLUX 50, using 3-D FEA (Ansys). Ansys uses adaptive meshing with built-in convergence for 3-D simulations; the mesh typically converged within 12 iterations. We find that for $\Pi_1 \geq 4$ the torque is nearly perfectly predicted by the 2-D model, for $4 > \Pi_1 > 1$ the torque is only slightly less than predicted by the 2-D model, and for $\Pi_1 \leq 1$ the torque can be substantially less than predicted by the 2-D model. For all values of Π_1, the values for Π_0/Π_1 from Fig. 6 are more accurate than the value obtained from 2-D FEA.

These results suggest that the "optimal" designs of Section IV may result in suboptimal performance for very small values of Π_1. For pancake-type radial magnetic torque couplers, it may be beneficial to further optimize for a specific

value of Π_1 in 3-D FEA, although it is uncertain if that would result in any improvement.

VI. Sensitivity to Changes in Fixed Parameters

In each of our design optimizations (i.e., using VACOFLUX 50 or 1010 Steel), we fixed the permanent-magnet material properties to a specific grade of NdFeB, and we (arbitrarily) fixed the air gap between the IR and OR to be 1% of the device's outer radius. The resulting optimal design was dependent on the resulting fixed Π_3, Π_8, and Π_9 values. We would like to explore how changing these parameters changes the optimal design. We performed a sensitivity analysis on these three Π terms, one term at a time, by adjusting the Π term slightly about the nominal value. When changing Π_8 and Π_9 we explicitly held μ_y and B_y constant and changed μ_m and $H_{\rm cm}$. It is important to note that μ_m appears in both Π_8 and Π_9; changing only Π_9 is accomplished by changing $H_{\rm cm}$, whereas changing only Π_8 requires a change in μ_m with a corresponding inverse change in $H_{\rm cm}$. When changing Π_3, we considered changes of $\pm 33\%$ of the nominal value, to reflect the potentially large change in the gap size. When changing Π_8 and Π_9, we considered changes of $\pm 1\%$ (approximately) of the nominal value, to reflect the relatively small change in the properties of different grades of permanent-magnet material. Each new design was optimized using the same procedure described in Section IV; the complete results of these optimizations are provided in Appendix B. Using these values, we used the central-difference method to compute the sensitivity values (i.e., partial derivatives) provided in Tables IV and V.

Using the result of the sensitivity analysis, we can explore how real changes in the fixed values impact the optimal design. Consider our nominal optimal design with VACOFLUX 50 as the soft-magnetic material. If we were to increase the gap size from 1% to 2% of the outer radius (i.e., $\Delta\Pi_3 = 0.01$), we would expect the nondimensional torque per length, Π_0/Π_1, to change from 1.15 to 1.03, which is a 10% reduction in torque due to this increase in gap size. However, the five geometric Π terms of the optimal design would each change by less than 2% (i.e., they are insensitive to changes in Π_3). If we instead consider a change in the permanent-magnet material from Grade N45SH NdFeB to Grade N48H—which has $\mu_m = 1.029\mu_0$ and $H_{\rm cm} = 1.075 \times 10^6$ A $\cdot$ m^{-1}, leading to simultaneous changes in Π_8 and Π_9—we find that we would expect a 20% increase in the optimal Π_6 and a 3% increase in the optimal Π_4, with negligible changes to all other geometric Π terms. We also find negligible changes in Π_0/Π_1, but because the permanent-magnet parameters also appear in the denominator of Π_0/Π_1, we conclude that this change in permanent-magnet material will result in a 7.8% increase in torque per volume.

We repeated the above two case studies, starting from our nominal optimal design with 1010 Steel as the soft-magnetic material. The increase in the gap size led to a 12% reduction in nondimensional torque, a 28% increase in optimal Π_6, a 7.7% decrease in optimal Π_4, a 2.2% increase in optimal Π_5, and negligible changes to the other geometric Π terms.

TABLE IV
Results of Sensitivity Analysis of Small Variations in Π_3 (i.e., Gap Size) and Π_8 and Π_9 (i.e., Permanent-Magnet Material), Using VACOFLUX 50 for the Soft-Magnetic Material

Π **Group**	$\frac{\partial}{\partial \Pi_3}$	$\frac{\partial}{\partial \Pi_8}$	$\frac{\partial}{\partial \Pi_9}$
$\frac{\Pi_0}{\Pi_1} = \frac{T}{\mu_m H_{cm}^2 R^2 L}$	-12	0.0	-0.59
$\Pi_2 = \frac{d_m}{R}$	-0.30	0.0	0.29
$\Pi_4 = \frac{d_s}{R}$	-0.15	1.4e-05	0.32
$\Pi_5 = \frac{d_y}{R}$	-0.11	7.1e-07	0.14
$\Pi_6 = E$	0.30	1.6e-04	0.27
$\Pi_7 = F$	-0.15	1.8e-05	0.18

TABLE V
Results of Sensitivity Analysis of Small Variations in Π_3 (i.e., Gap Size) and Π_8 and Π_9 (i.e., Permanent-Magnet Material), Using 1010 Steel for the Soft-Magnetic Material

Π **Group**	$\frac{\partial}{\partial \Pi_3}$	$\frac{\partial}{\partial \Pi_8}$	$\frac{\partial}{\partial \Pi_9}$
$\frac{\Pi_0}{\Pi_1} = \frac{T}{\mu_m H_{cm}^2 R^2 L}$	-13.6	0.0	-0.32
$\Pi_2 = \frac{d_m}{R}$	-0.30	0.0	0.0
$\Pi_4 = \frac{d_s}{R}$	-0.76	2.3e-04	-0.095
$\Pi_5 = \frac{d_y}{R}$	0.11	2.8e-04	-0.10
$\Pi_6 = E$	5.0	1.1e-03	-0.25
$\Pi_7 = F$	0.61	1.3e-04	-0.22

The change in the permanent-magnet material led to a negligible change in Π_0/Π_1, which again corresponds to a 7.8% increase in torque per volume. It led to large changes in four of the five geometric Π terms: a 55% increase in Π_4, a 130% increase in Π_5, a 148% increase in Π_6, and a 3.1% increase in Π_7.

It is important to note that, in the design process of a new device, one would be well-advised to use an application of the sensitivity study to initialize a new gradient-based optimization. Application of the sensitivity study, which is based on assumptions of linearity, is likely to result in a design that is close to optimal, but due to nonlinearities, would likely evolve somewhat from the initialization.

VII. Discussion

For variable-reluctance torque couplers, we found that the optimal design (of the viable candidates) was the one with the largest number of IR magnets. As a result, the development of Section III-B can be subsumed by a simple relationship

TABLE VI

OPTIMAL DESIGNS FOR SMALL VARIATIONS IN Π_3, Π_8, AND Π_9, USING VACOFLUX 50 FOR THE SOFT-MAGNETIC MATERIAL. NOMINAL VALUES ARE $\Pi_3 = 0.01$, $\Pi_8 = 14\,300$, AND $\Pi_9 = 1.74$

Π Group	Nominal Design	$\Pi_3 = 0.0066$	$\Pi_3 = 0.013$	$\Pi_8 = 14200$	$\Pi_8 = 14480$	$\Pi_9 = 1.7240$	$\Pi_9 = 1.7579$
$\frac{\Pi_0}{\Pi_1} = \frac{T}{\mu_m H_{cm}^2 R^2 L}$	1.15	1.17	1.09	1.14	1.14	1.15	1.13
$\Pi_2 = \frac{d_m}{R}$	0.296	0.297	0.295	0.296	0.296	0.295	0.296
$\Pi_4 = \frac{d_s}{R}$	0.109	0.100	0.099	0.101	0.105	0.099	0.110
$\Pi_5 = \frac{d_y}{R}$	0.0573	0.0514	0.0507	0.0517	0.0519	0.0511	0.0557
$\Pi_6 = E$	0.185	0.179	0.181	0.161	0.207	0.166	0.175
$\Pi_7 = F$	0.978	0.977	0.976	0.980	0.985	0.971	0.977

TABLE VII

OPTIMAL DESIGNS FOR SMALL VARIATIONS IN Π_3, Π_8, AND Π_9, USING 1010 STEEL FOR THE SOFT-MAGNETIC MATERIAL. NOMINAL VALUES ARE $\Pi_3 = 0.01$, $\Pi_8 = 2025$, AND $\Pi_9 = 1.62$

Π Group	Nominal Design	$\Pi_3 = 0.0066$	$\Pi_3 = 0.013$	$\Pi_8 = 2005$	$\Pi_8 = 2045$	$\Pi_9 = 1.6067$	$\Pi_9 = 1.6383$
$\frac{\Pi_0}{\Pi_1} = \frac{T}{\mu_m H_{cm}^2 R^2 L}$	1.11	1.17	1.08	1.12	1.12	1.12	1.11
$\Pi_2 = \frac{d_m}{R}$	0.296	0.293	0.295	0.296	0.296	0.296	0.296
$\Pi_4 = \frac{d_s}{R}$	0.099	0.114	0.095	0.101	0.110	0.103	0.100
$\Pi_5 = \frac{d_y}{R}$	0.0511	0.0648	0.0521	0.0514	0.0625	0.0545	0.0512
$\Pi_6 = E$	0.176	0.161	0.212	0.157	0.199	0.174	0.166
$\Pi_7 = F$	0.978	0.976	0.981	0.974	0.979	0.984	0.977

(which has been assumed previously [1], [2])

$$N_{\mathrm{IR}} = N_{\mathrm{OR}} = Z. \tag{7}$$

In the optimal variable-reluctance design [see Fig. 5(b)], the IR magnets take up most of the IR, with a design that may be challenging/impractical to fabricate. We explored the effect of decreasing the thickness of the IR magnets and increasing the radius of the IR core by an equivalent amount, to make a design that is easier to fabricate. Although the optimal nondimensional IR magnetic thickness is $\Pi_2 = 0.787$, we found that it could be reduced to a value of $\Pi_2 = 0.333$ with only a 1% reduction in torque.

In the optimal permanent-magnet torque coupler we found that the optimization resulted in a large rotor radius. This large rotor radius resulted in a thin highly saturated yoke, specifically between adjacent OR magnets, as shown in Fig. 2. Additionally, the IR core, which consists of entirely soft magnetic material is utilized at only a fraction of the entire IR core's radial depth. Designers can remove the IR core and replace it with a nonmagnetic shaft with a nondimensional radius of up to 0.25, or alternatively the IR core can be removed to reduce inertia, without reduction in torque.

In prior studies involving optimization of magnetic torque couplers, it has been typical to consider the volumetric torque density as the figure of merit, which may take the form of torque normalized by package-size volume (i.e., $\pi R^2 L$) or torque normalized by the volume of the magnetic material used. In our formulation using dimensional analysis, we arrived at a nondimensional output that was normalized by $R^2 L$, maintaining the intuitive proportionality to volume, but that also had the advantage of being properly normalized by the permanent magnet's material properties.

It is important to note that our analysis only optimizes within the parameterization defined in Fig. 1. Our optimization does not allow for the IR/OR magnets or OR teeth to fundamentally change shape.

VIII. CONCLUSION

Using the Buckingham Π theorem, we found that, although torque in a radial magnetic torque coupler is a function of 12 independent parameters, a nondimensional torque term can be expressed as a function of just nine independent nondimensional terms. Using 2-D FEA, we parameterically designed the cross-section geometry for a radial magnetic torque coupler with eight stable magnetic equilibria (i.e., 45° of rotation between stable equilibria), but with a methodology that generalizes to other values, and we found the resulting peak torque, nondimensionalized by the size of the device and the energy product of the permanent-magnet material. Finally, using 3-D FEA, we determined that the results of the 2-D-FEA optimization are accurate for a torque coupler with an axial length that is longer than its diameter.

$$A^T = \begin{array}{c} \\ T \\ L \\ R \\ d_m \\ d_g \\ d_s \\ d_y \\ E \\ F \\ \mu_y \\ B_y \\ \mu_m \\ H_{\text{cm}} \end{array} \begin{array}{c} \begin{array}{ccc} \text{m} & \text{N} & \text{A} \end{array} \\ \begin{bmatrix} 1 & 1 & 0 \\ 1 & 0 & 0 \\ 1 & 0 & 0 \\ 1 & 0 & 0 \\ 1 & 0 & 0 \\ 1 & 0 & 0 \\ 1 & 0 & 0 \\ 0 & 0 & 0 \\ 0 & 0 & 0 \\ 0 & 1 & -2 \\ -1 & 1 & -1 \\ 0 & 1 & -2 \\ -1 & 0 & 1 \end{bmatrix} \end{array}, \quad B = \begin{array}{c} \\ T \\ L \\ R \\ d_m \\ d_g \\ d_s \\ d_y \\ E \\ F \\ \mu_y \\ B_y \\ \mu_m \\ H_{\text{cm}} \end{array} \begin{array}{c} \begin{array}{cccccccccc} \Pi_0 & \Pi_1 & \Pi_2 & \Pi_3 & \Pi_4 & \Pi_5 & \Pi_6 & \Pi_7 & \Pi_8 & \Pi_9 \end{array} \\ \begin{bmatrix} 1 & 0 & 0 & 0 & 0 & 0 & 0 & 0 & 0 & 0 \\ 0 & 1 & 0 & 0 & 0 & 0 & 0 & 0 & 0 & 0 \\ -3 & -1 & -1 & -1 & -1 & -1 & 0 & 0 & 0 & 0 \\ 0 & 0 & 1 & 0 & 0 & 0 & 0 & 0 & 0 & 0 \\ 0 & 0 & 0 & 1 & 0 & 0 & 0 & 0 & 0 & 0 \\ 0 & 0 & 0 & 0 & 1 & 0 & 0 & 0 & 0 & 0 \\ 0 & 0 & 0 & 0 & 0 & 1 & 0 & 0 & 0 & 0 \\ 0 & 0 & 0 & 0 & 0 & 0 & 1 & 0 & 0 & 0 \\ 0 & 0 & 0 & 0 & 0 & 0 & 0 & 1 & 0 & 0 \\ 0 & 0 & 0 & 0 & 0 & 0 & 0 & 0 & 1 & 0 \\ 0 & 0 & 0 & 0 & 0 & 0 & 0 & 0 & 0 & 1 \\ -1 & 0 & 0 & 0 & 0 & 0 & 0 & 0 & -1 & -1 \\ -2 & 0 & 0 & 0 & 0 & 0 & 0 & 0 & 0 & -1 \end{bmatrix} \end{array} \tag{8}$$

APPENDIX A
APPLICATION OF BUCKINGHAM Π THEOREM

Our choice of dimensionless Π groups provided in Table I is not unique, but we can check that our proposed Π groups are valid by constructing two matrices. The first is a matrix A^T, where each row corresponds to a parameter, each column corresponds to a dimension, and each element contains the power of the dimensions in the respective parameters. The second is a matrix B where the rows again correspond to the parameters (ordered as in A^T), each column corresponds to a Π group, and each element contains the power of the parameters in the respective Π groups. A valid set of Π groups is one in which B has full column rank and AB is a zero matrix. It can be shown that the matrices provided in (8), as shown at the top of the page, which correspond to the Π groups in Table I, meet this requirement, and thus our Π groups are valid.

APPENDIX B
SIMULATION RESULTS USED IN SENSITIVITY ANALYSIS

In Section VI we described a sensitivity analysis around our two nominal optimal designs. The process involved making small changes to each of Π_3, Π_8, and Π_9, one at a time, and then rerunning the design optimization. The results of this process for VACOFLUX 50 are provided in Table VI, and the results for 1010 Steel are provided in Table VII. These values were then used, using the central-difference method, to compute the partial-derivative values reported in Tables IV and V, respectively.

REFERENCES

[1] M. H. Nagrial, "Analysis and performance of variable reluctance (VR) torque coupler," in *Proc. IEEE Conf. Ind. Autom. Control Emerg. Technol. Appl.*, May 1995, pp. 136–139.

[2] M. H. Nagrial, "Finite element analysis and design of variable reluctance (VR) torque coupler," in *Proc. 2nd Int. Conf. Power Electron. Drive Syst.*, May 1997, pp. 252–254.

[3] R. M. Hornreich and S. Shtrikman, "Optimal design of synchronous torque couplers," *IEEE Trans. Magn.*, vol. MAG-14, no. 5, pp. 800–802, Dec. 1978.

[4] W. Wu, H. C. Lovatt, and J. B. Dunlop, "Analysis and design optimisation of magnetic couplings using 3D finite element modelling," *IEEE Trans. Magn.*, vol. 33, no. 5, pp. 4083–4085, Sep. 1997.

[5] J.-Y. Choi, H.-J. Shin, S.-M. Jang, and S.-H. Lee, "Torque analysis and measurements of cylindrical air-gap synchronous permanent magnet couplings based on analytical magnetic field calculations," *IEEE Trans. Magn.*, vol. 49, no. 7, pp. 3921–3924, Jul. 2013.

[6] E. P. Furlani, R. Wang, and H. Kusnadi, "A three-dimensional model for computing the torque of radial couplings," *IEEE Trans. Magn.*, vol. 31, no. 5, pp. 2522–2526, Sep. 1995.

[7] E. P. Furlani, "Analysis and optimization of synchronous magnetic couplings," *J. Appl. Phys.*, vol. 79, no. 8, pp. 4692–4694, 1996.

[8] J. Charpentier and G. Lemarquand, "Optimal design of cylindrical air-gap synchronous permanent magnet couplings," *IEEE Trans. Magn.*, vol. 35, no. 2, pp. 1037–1046, Mar. 1999.

[9] W. Y. Lin, L. P. Kuan, W. Jun, and D. Han, "Near-optimal design and 3-D finite element analysis of multiple sets of radial magnetic couplings," *IEEE Trans. Magn.*, vol. 44, no. 12, pp. 4747–4753, Dec. 2008.

[10] R. Ravaud, V. Lemarquand, and G. Lemarquand, "Analytical design of permanent magnet radial couplings," *IEEE Trans. Magn.*, vol. 46, no. 11, pp. 3860–3865, Nov. 2010.

[11] Z. Meng, Z. Zhu, and Y. Sun, "3-D analysis for the torque of permanent magnet coupler," *IEEE Trans. Magn.*, vol. 51, no. 4, Apr. 2015, Art. no. 8002008.

[12] G. I. Barenblatt, *Scaling, Self-Similarity, Intermediate Asymptotics*. Cambridge, U.K.: Cambridge Univ. Press, 1996.

[13] E. P. Furlani, *Permanent Magnet and Electromechanical Devices: Materials, Analysis, and Applications*. San Diego, CA, USA: Academic, 2001.

[14] N. Bianchi and S. Bolognani, "Design techniques for reducing the cogging torque in surface-mounted PM motors," *IEEE Trans. Ind. Appl.*, vol. 38, no. 5, pp. 1259–1265, Sep./Oct. 2002.

[15] D. C. Meeker. *Finite Element Method Magnetics*. Accessed: Jun. 21, 2021. [Online]. Available: https://www.femm.info